CrystEngComm

Accepted Manuscript

ROYAL SOCIETY OF CHEMISTRY

www.rsc.org/crystengcomm

Graphical Abstract

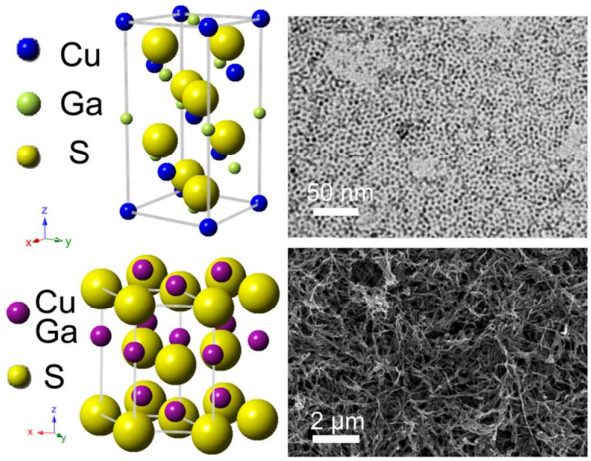

We report the selective synthesis of $CuGaS_2$ nanostructures of different sizes (3.0 nm to 10.9 nm), phases (chalcopyrite and wurtzite) and morphologies (nanocrystals and nanowires) in hot-solvent synthesis.

CrystEngComm RSCPublishing

ARTICLE

Cite this: DOI: 10.1039/x0xx00000x

Selective Synthesis of Cupper Gallium Sulfide ($CuGaS_2$) Nanostructures of Different Sizes, Crystal Phases, and Morphologies

Received ooth January 2012,
Accepted ooth January 2012

DOI: 10.1039/x0xx00000x

www.rsc.org/

Shu-Hao Chang,[†] Bo-Cheng Chiu,[†] Tzu-Lun Gao, Shao-Lou Jheng, and Hsing-Yu Tuan[*]

$CuGaS_2$ nanostructures with different sizes, phases and morphologies were prepared. Chalcopyrite $CuGaS_2$ nanocrystals with sizes ranging from 3.0 nm to 10.9 nm were synthesized using $GaCl_3$, CuCl, and elemental sulfur as the precursors at temperatures ranging from 180 to 240 °C in hot-solvent synthesis. The $CuGaS_2$ nanocrystals show size-dependent optical absorption and photoluminescence properties, exhibiting quantum confinement effect. Wurtzite $CuGaS_2$ nanostructures could be synthesized by replacing elemental sulfur with thiourea as the S source. We find that the amount of oleylamine (OLA) significantly affects the morphologies of $CuGaS_2$ nanostructures: $CuGaS_2$ nanowires tend to form while the amount of OLA in the reaction decreased. The growth mechanism of $CuGaS_2$ nanowires is proposed based on the experimental observation of morphology evolution from 130 to 240 °C.

1. Introduction

I-III-VI_2 chalcopyrite semiconductor materials such as $CuInS_2$, $CuInSe_2$ and $CuInGaSe_2$ are receiving significant attention as thin film absorbing layers in photovoltaic devices due to their promising characteristics, including suitable direct energy gap energies to the solar spectrum, high absorption coefficient (10^5 cm^{-1}) with good electrical stability and good radiation stabilities.[1-3] Nano-sized I-III-VI_2 ternary compounds have been particularly influential in photovoltaics,[4-8] energy storage fields[9,10] and medical imaging applications.[11] The attractive spot of these nanomaterials is that they can be directly implemented in the advanced applications through solution-based deposition process without high-vacuum equipment. This greatly reduces the fabrication cost[12-15] and is the future trend to photovoltaic manufacturing procedure for mass production.[16] In recent years, many synthetic techniques of I-III-VI_2 nanocrystals, such as solvothermal reactions,[17,18] hot-solvent synthesis,[19-23] and seed catalytic growth[24] have been intensively investigated. Synthetic methods coupled with resolved mechanism are therefore of special important.

Size, phase and shape of nanocrystals closely interact with the nanocrystal properties.[25] Some interesting works have been done in the field of nanomaterial synthesis. For example, Yarema et al. controlled the size of $CuInSe_2$ nanocrystals between 2.7 nm and 7.9 nm by varying reaction time and reaction temperature.[26] On the other hand, shape control has raised interest for the fabrication of semiconductor nanocrystalssince due to its correlation with physical properties or chemical reactivity. For instance, one-dimensional (1D) nanomaterials, (e.g. nanorods and nanowires) have been observed to exhibit different optical properties, such as emission polarization.[27] Although 1D nanostructures can be fabricated through a wide range of advanced nanolithography, including electron-beam and focused-ion-beam writing, in order to achieve low-cost, large-scale production, new synthetic techniques should be developed. For nanocrystal synthesis, three strategies are usually applied to fabricate 1D nanostructure in chemical synthesis: i) template-assisted anisotropic growth. ii) capping reagents-guided kinetic anisotropic growth.[28] iii) Oriented attachment-mediated assembly of nanoparticles to nanowires. [29-33] Further, materials with different phases also exhibit distinct properties. For example, wurtzite phase of I-III-VI_2 materials exhibit different optical properties since they offer higher flexibility of stoichiometry control due to random distribution of I and III groups of ions, which may be advantageous for solar cell applications.[34-35]

$CuGaS_2$ nanocrystals has a direct bandgap of 2.49 eV with high absorption coefficient (10^5~10^6 cm^{-1}).[36,37] However, the reactivity of Ga precursor is different from that of other compositions, leading to free gallium nuclei in the reaction.[35] There are some reports on the synthesis of $CuGaS_2$ nanocrystals through hydrothermal and solvothermal methods. However, most of nanoparticles appear in the form of large crystallities.[38,39] In the very recently, wurtzite phase of $CuGaS_2$ nanocrystals has been synthesized.[37,40] However, there still lacks studies to systematically control the synthesis of $CuGaS_2$ nanomaterials.

In this report, chalcopyrite $CuGaS_2$ nanocrystals with diameters ranging from 3.0 to 10.9 nm were obtained using $GaCl_3$, CuCl, and elemental sulfur as the precursors at temperatures ranging from 180 to 240 °C in hot-solvent synthesis. Size-dependent optical properties of $CuGaS_2$ nanocrystals are observed from the optical absorption and photoluminescence (PL) spectra, showing their quantum confinement effect. On the other hand, by changing the sulfur

source from sulfur powder to thiourea, wurtzite $CuGaS_2$ nanocrystals were obtained. Further, by decreasing the amount of oleylamine (OLA) in the synthesis, wurtzite nanowires were formed. This study represents a systematic approach to selectively obtain $CuGaS_2$ nanostructures with different sizes, phases, and morphologies.

2. Experimental details

Materials.

Copper(I) chloride (CuCl, 99.99%), gallium(III) chloride ($GaCl_3$, 99.99%), oleylamine (OLA, 97%) and sulfur powder (S, 99.99%), 1-dodecanethiol (DDT, 98%), thiourea, dodecylamine (DDA) and ethanol (99.5%) were purchased from Aldrich. All chemicals were used without further purification.

Synthesis of 5.6 nm to 10.9 nm chalcopyrite type $CuGaS_2$ nanocrystals

Chalcopyrite $CuGaS_2$ nanocrystals were synthesized by the following procedure. OLA solution, copper(I) chloride (CuCl, 0.5 mmol) and gallium chloride ($GaCl_3$, 0.5 mmol) added to OLA (10 mL), was heated to 240 ^oC with argon bubbling. The reaction was initiated by the rapid injection of sulfur precursor (1.0 mmol of sulfur powder dissolved into 2 mL of OLA) into the hot solution. After 1 hr, the resulting solution was cooled to room temperature and treated with ethanol to precipitate orange flocculates that were subsequently separated by centrifugation. The post-treatment is essential for further narrowing the size distribution of $CuGaS_2$ nanocrystals. Anhydrous ethanol was added dropwise to $CuGaS_2$ nanocrystal solution until opalescence persisted upon shaking or sonication. Separation of supernatant by centrifugation produced a precipitate enriched with the largest crystallites in the sample. The same procedures were repeated several times for subsequent supernatant containing smaller nanoparticles until the clear solution was noted. Each precipitate can disperse in nonpolar organic solvents, including hexane, toluene and chloroform.

Synthesis of 3 nm chalcopyrite $CuGaS_2$ nanocrystals

In a typical synthesis of 3 nm $CuGaS_2$ nanoparticles, gallium chloride (0.5 mmol) is mixed with copper(I) chloride (0.5 mmol) and DDT (4 mL) in a three-necked flask containing OLA (6 mL). The mixture was purged with argon for 30 min. The flask was heated to 130 ^oC for 30 min until a transparent yellow solution formed. The temperature was then raised to 180 ^oC. Sulfur powder (1 mmol) dissolved in 2 mL of the OLA was rapidly injected into the reaction flask, then the color of the solution progressively changes from transparent yellow to claret-red indicating nucleation and subsequent growth of $CuGaS_2$ nanocrystals. After 10 min of heating, the reaction mixture was cooled to room temperature using a water bath. The crude solution was mixed with equal volume of hexane and excess ethanol to allow flocculates form. The nanoparticles were isolated by centrifugation at 8000 rpm for 10 min. The precipitated nanoparticles can be redispersed in toluene and washed twice with the same way to discard remaining capping agents. The nanocrystals were then redispersed in 10 mL of hexane and centrifuged at 7000 rpm for 5 min to remove poorly capped nanocrystals and large particulates, which settled out during centrifugation. The well-capped nanocrystals can be dispersed in hexane or other organic solvents.

Syntheisis of wurtzite type $CuGaS_2$ nanocrystals and nanowires

In a typical synthesis of wurtzite $CuGaS_2$ nanocrystals, 0.5 mmol of CuCl, 0.5 mmol of $GaCl_3$, 1 mmol of thiourea and 24 mL of OLA were added to a 50 mL three-neck flask with stopcock valves in a nitrogen-filled glovebox. The stopcock valve was closed before removing the flask from the glovebox. It was connected to a Schlenk line and placed on a heating mantle. Then, the reaction mixture was heated to 240 ^oC under vigorous magnetic stirring. After 1 hr, the crude solution was cooled to room temperature using a water bath and then centrifuged at 7000 rpm for 5 min with 10 mL hexane to remove large clusters. The supernatant of nanoparticles can be separated by further centrifugation at 8000 rpm for 10 min with 10 mL hexane and 15 mL ethanol.

Wurtzite $CuGaS_2$ nanowires were synthesized with the same procedure but using 12 mL of OLA instead of 24 mL. The crude solution was centrifuged at 8000 rpm for 10 min with 10 mL hexane and 15 mL ethanol to remove unreacted precursors. The purified nanoparticles and nanowires were redispersed in toluene for further characterization without any size sorting.

Characterization

The morphologies of the as-grown $CuGaS_2$ nanocrystals were analysed by transmission electron microscopy (TEM) and high resolution TEM (HR-TEM). A Topcon EM002B electron microscope operating at 200 kV was used for TEM. Samples were prepared by placing a drop of a dilute dispersion of nanocrystal solution on the surface of a copper grid (300 mesh) coated with amorphous carbon film. The crystal structures were determined using X-ray powder diffraction (XRD) on a Rigaku 300 Rotaflex diffractometer operating in the Bragg configuration using Cu Kα radiation. The accelerating voltage was set at 250 kV with a 200 milliamp flux. Scatter and diffraction slits of 0.50^o and a 0.15-mm collection slit were used. For elemental analysis, The Tecnai F30ST (FEI) instrument with a field emission gun was equipped with an Energy-Dispersive Spectroscopy (EDS) spectrometer for EDS analysis. UV-Vis spectra were recorded on a Hitachi U-4100 UV-Vis-NIR spectrophotometer at room temperature. PL spectra were taken using a Spex Fluorolog-3 fluorometer.

3. Results and discussion

3.1 Synthesis of chalcopyrite $CuGaS_2$ nanocrystals

For ternary I-III-VI_2 nanocrystal synthesis, how to balance the reaction activity of each reagent needs to be greatly considered to avoid the formation of heterostructures, as core/shell, composite structure, or even two compounds. Metal chlorides dissolve in OLA as reactants was used to prepare chalcopyrite-type $CuInS_2$, $CuInSe_2$, $CuIn(S_xSe_{1-x})_2$ and $Cu(In_{1-x}Ga_x)(S_ySe_{1-y})_2$ nanoparticles.[21,22] OLA serves as a good surfactant for forming metal chalcogenide nanocrystals and could reduce the reactivity difference between Cu, In, Ga, Se and S reactants. Chalcopyrite-type $CuGaS_2$ nanocrystals were synthesized through a thermal decomposition method. $GaCl_3$ dissolved in OLA could be directly used as a Ga source. Sulfur powder dissolved in OLA with a short duration of sonication was injected into the preheated metal halides/OLA solution and kept at 240 ^oC for 1 hr. by adding CuCl, $GaCl_3$ and S powder as Cu, Ga and S source to the reaction:

$$CuCl+GaCl_3+S \xrightarrow{OLA,240\ ^oC} CuGaS_2 \text{ nanocrystals+byproducts} \quad (1)$$

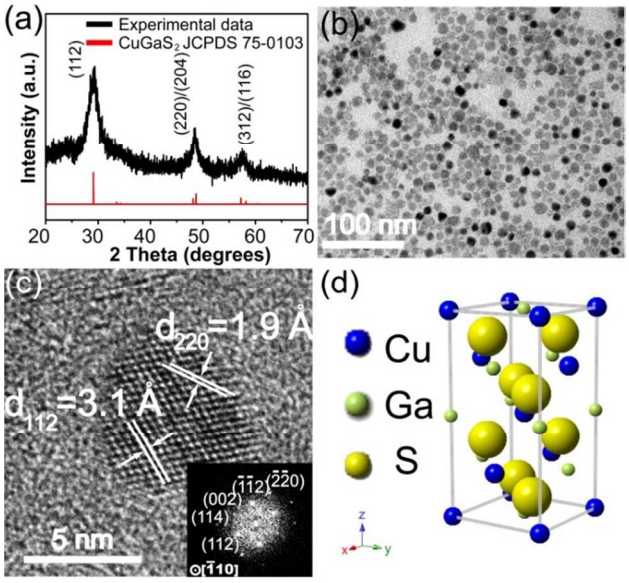

Figure 1. Chalcopyrite $CuGaS_2$ nanocrystals synthesized from CuCl, $GaCl_3$, and S with OLA as surfactant at 240 ^oC for 1 hr. (a) XRD, (b) TEM, (c) HRTEM and corresponding FFT image and (d) simulated unit cell of chalcopyrite $CuGaS_2$.

Figure 1a shows the XRD pattern of the product, in which only chalcopyrite $CuGaS_2$ peaks are observed without impurity peak. In the previous synthesis of $CuInS_2$ nanocrystals, the difference between chalcopyrite phase and zincblende phase is very small, but the $CuInS_2$ nanocrystals with zincblende phase usually have a diffraction peak of (200).[41-43] In our work, the absence of this peak in the XRD patterns of $CuGaS_2$ nanocrystals can be considered as an evidence for the chalcopyrite phase. The TEM image of $CuGaS_2$ nanocrystals (Figure 1b) shows that the nanocrystals are in the shape of sphere, but with relatively broad size distribution. HRTEM (Figure 1c) of one nanocrystals shows high crystallinity nature; the lattice fringes of $CuGaS_2$ nanoparticles shows a spacing of d = 0.19 nm and d = 0.31 nm, which corresponds to the (220) and (112) lattice plane of the chalcopyrite of $CuGaS_2$. The FFT image of the HRTEM image along the zone axis of [-110] direction is also consistent with chalcopyrite $CuGaS_2$. The corresponding $CuGaS_2$ crystal structure is shown in Figure 1d.

In order to obtain nanoparticles with more uniform sizes, a precipitation procedure was applied to narrow down the size distribution. Ethanol, served as polar anti-solvent, was introduced to the concentrated $CuGaS_2$ solution dropwise until the $CuGaS_2$ nanocrystals started to precipitate, resulting in opalescence and turbid solution. The reason for this phenomenon is that the decrease of ligand-solvent interaction causes particles unstable in solution. Further, the different sizes of $CuGaS_2$ nanoparticles can be separated by centrifugation. With several times of isolation procedures, different sizes of $CuGaS_2$ nanoparticles can be obtained. Figure 2 shows TEM images of $CuGaS_2$ nanoparticles at each size-selective precipitation step and the $CuGaS_2$ nanocrystals with the nearly monodisperse nanocrystals were obtained. The average diameters of the three samples are 10.9±0.9 nm, 7.9±1.1 nm, and 5.6±0.7 nm, respectively.

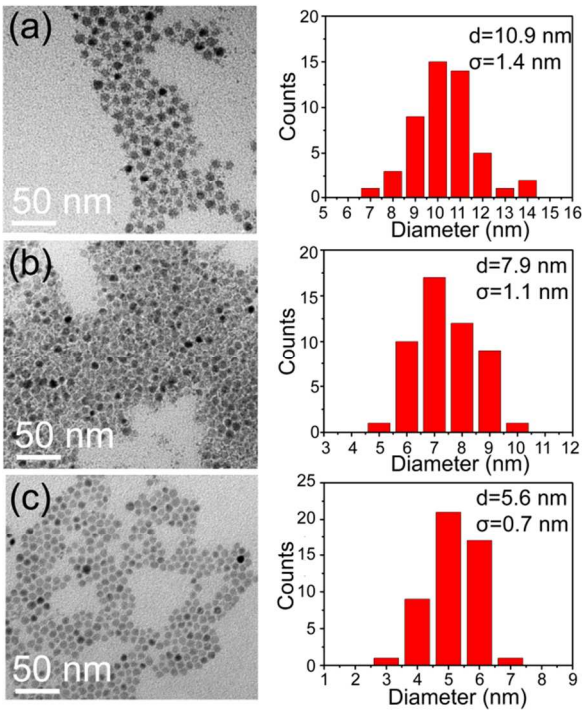

Figure 2. TEM image and size distribution histogram of chalcopyrite $CuGaS_2$ nanoparticles with average size of (a) 10.9 ±1.4 nm (b) 7.9±1.1 nm (c) 5.6±0.7 nm.

On the other hand, we find that using a combination of DDT and OLA in the reaction can obtain smaller $CuGaS_2$ nanocrystals. It was noticed that thiols can serve as the stabilizing ligand and the solvent in the reaction. It can also play the role of the sulfur source, which forms thiolates with metal ions.[44] Figure 3a shows the XRD pattern of $CuGaS_2$ nanocrystal prepared with 8 mL OLA and 4 mL DDT. The diameter of nanocrystals is approximately 3.0±0.4 nm. Both XRD and HRTEM confirmed that the nanocrystals are crystalline with chalcopyrite $CuGaS_2$ structure. The d-spacing observed in HRTEM image is also consistent with chalcopyrite $CuGaS_2$.

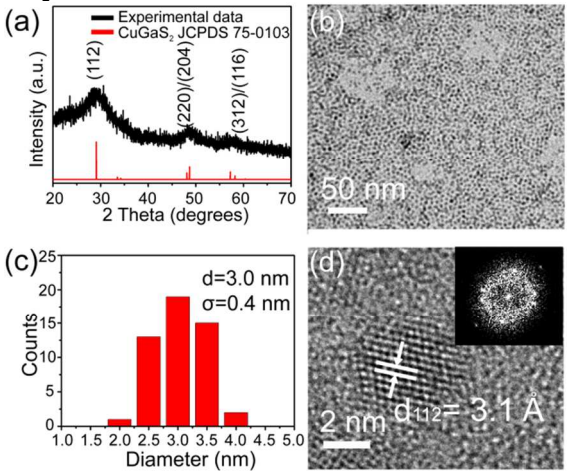

Figure 3. OLA and DDT capped $CuGaS_2$ chalcopyrite nanocrystals synthesized at 180 ^oC for 10 min. The nanoparticles with the average size of 3.0±0.4 nm were obtained. (a) XRD pattern (b) The TEM image (c) size distribution histogram and (d) HRTEM image.

Figure 4a shows the UV-Vis absorbance spectra of the four samples of different sizes of chalcopyrite $CuGaS_2$ nanoparticles dispersed in toluene. The absorption edge shows the blue-shift upon decreasing the size of the nanocrystals, exhibiting a quantum dot-like behavior. The nature of the broad emission peak was completely observed (Figure 4b), and the PL spectra match well with absorption spectra for the samples after the size sorting. It also shows blue-shifted while the size decreased in the PL spectra. In figure 4c, the experiment values are consistent with theoretical calculation in the size range below 6 nm.[45]

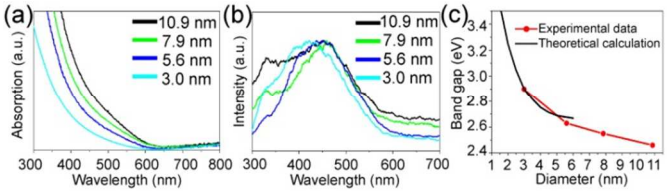

Figure 4. (a) UV-Vis absorbance spectra and (b) corresponding PL of different sizes of chalcopyrite $CuGaS_2$ nanocrystals. (c) The comparison of optical band gap with theoretical band gap.[45]

3.2 Synthesis of wurtzite $CuGaS_2$ nanocrystals

Wurtzite $CuGaS_2$ nanoparticles can be synthesized using thiourea as a sulfur source with OLA. The XRD pattern (Figure 5a) shows the characteristic of hexagonal cell with space group of P63mc. The cell parameters and corresponding structural parameters are shown in Table 1.

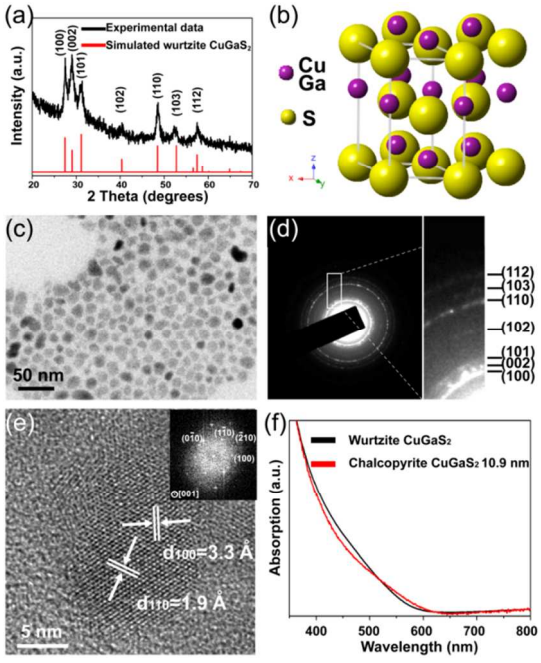

Figure 5. Wurtzite $CuGaS_2$ nanocrystals synthesized from CuCl, $GaCl_3$ and thiourea with 24 mL OLA as surfactant at 240 ^oC for 1 hr. (a) XRD, (b) crystal structure of wurtzite crystal structure. Note that Cu and Ga atoms occupy the same position. (c,d) TEM and corresponding SAED, (e) HRTEM and corresponding FFT, and (f) UV-Vis spectra (comparison to chalcopyrite $CuGaS_2$) of wurtzite $CuGaS_2$ nanocrystals.

The as-synthesized wurtzite $CuGaS_2$ nanocrystals are polydisperse with a mean diameter of 29.9±6.6 nm, as determined by TEM analysis (Figure 5c). Also, no other crystal phases were observed by SAED analysis (Figure 5d). The HRTEM image of an apparent single crystalline particle with the (100) and (110) lattice planes, displaying a d-spacing of 0.33 nm and 0.19 nm as shown in Figure 5e. The optical spectrum of wurtzite $CuGaS_2$ nanocrystals is similar to the optical absorption spectra of chalcopyrite $CuGaS_2$ nanoparticles (Figure 5f). Band gap of the wurtzite $CuGaS_2$ nanocrystals was determined from the onset of the UV-Vis absorption spectrum to be Eg = 2.47 eV, while bulk chalcopyrite $CuGaS_2$ has a reported band gap between 2.4-2.5 eV. EDS analysis (Supporting Information Figures S3) indicates that the chemical composition of the product is composed of Cu, Ga and S with mole ratio of 1.06:1:2.24, which is close to the stoichiometric compositions of $CuGaS_2$.

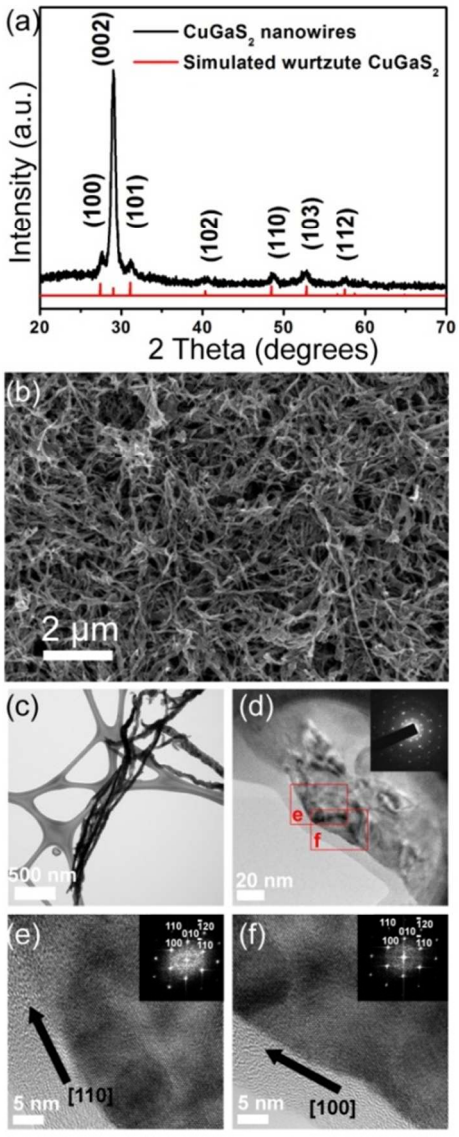

Figure 6. Wurtzite $CuGaS_2$ nanowires synthesized from CuCl, $GaCl_3$ and thiourea with 12 mL OLA as surfactant at 240 ^oC for 1 hr. (a) XRD pattern, and (b) SEM image, (c,d) TEM image, and (e,f) HRTEM of wurtzite $CuGaS_2$ nanowires.

Table 1. Crystal parameters of wurtzite $CuGaS_2$

Atom	Wyck.	x /a	y/b	z/c
Cu	2b	1/3	2/3	0
Ga	2b	1/3	2/3	0
S	2b	1/3	2/3	0.3752

Decreasing the amount of OLA favours the formation of nanowires. When the amount of OLA decreased from 24 mL to 12 mL, $CuGaS_2$ nanowires were produced as shown in Figure 6. All solid nanowires were found to be highly-crystalline with wurtzite crystal structure. The average length of the nanowires is typically over 4 μm, while the average diameter can be formed in the range between 50 to 100 nm. The HRTEM images (Figure 6e and 6f) and their corresponding SAED patterns (inset of Figure 6e and 6f) are analyzed. Two nanowire sections with the same FFT are shown. The FFTs can be indexed alone the [001] zone axis and two directions along [110] and [100] can be observed. These data suggest that the curvature of $CuGaS_2$ nanowires were formed by oriented attachment.

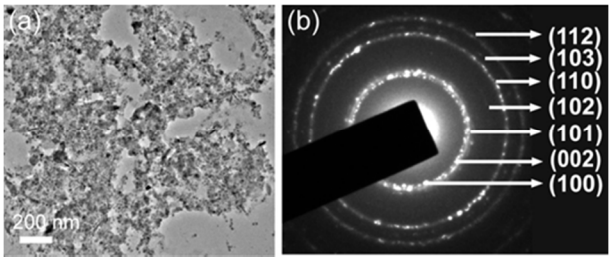

Figure 7. Wurtzite $CuGaS_2$ nanocrystals synthesized from CuCl, $GaCl_3$ and thiourea with 12 mL DDA as surfactant at 240 ^oC for 1 hr. (a) TEM image and (b) corresponding SAED pattern of wurtzite $CuGaS_2$ nanoparticles capped by DDA.

When an equal volume of DDA was substituted for OLA under otherwise identical conditions, the wurtzite phase of $CuGaS_2$ nanocrystals and nanorods (W<100 nm, L<200 nm) were produced without any nanowires formed. This suggests that the presence of different chains of the primary amine has an influence on product morphology.

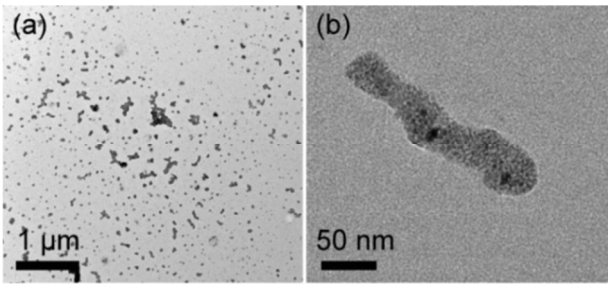

Figure 8. TEM image of wurtzite $CuGaS_2$ nanorods synthesized from 0.1 mmol CuCl, 0.1 mmol $GaCl_3$ and 0.2 mmol thiourea (1/5 of the typical reactant concentration) with 12 mL OLA as surfactant at 240 ^oC for 1 hr.

In addition, further experiments indicate that the reactant concentration strongly influence the nanowire formation. When the concentration of reactants was decreased to the one-fifth of the typical nanowire growth solution, no nanowires were found. Figure 8a exhibits the typical morphologies of short wires and its magnified image was shown in Figure 8b. Further observation reveals that the structure of short wires comprises several small wurtize $CuGaS_2$ nanoparticles.

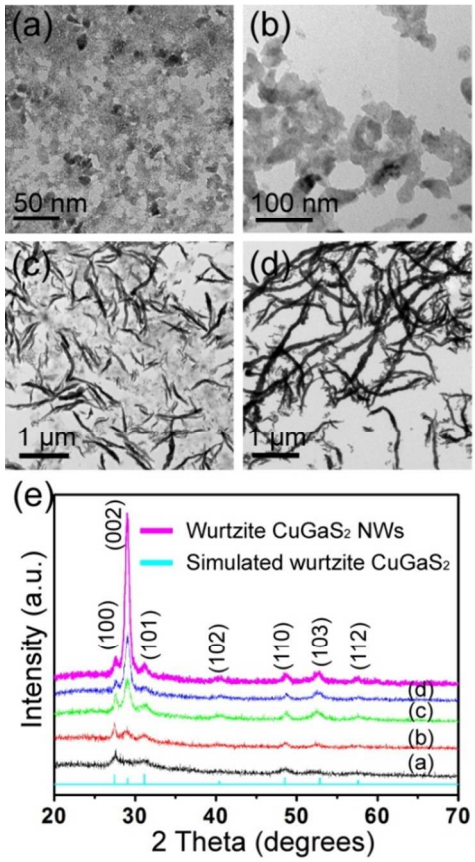

Figure 9. TEM image of wurtzite $CuGaS_2$ nanocrystals synthesized from CuCl, $GaCl_3$ and thiourea with 12 mL OLA as surfactant at (a) 130 ^oC (b) 180 ^oC (c) 200 ^oC (d) 240 ^oC for 5 min, (e) and their corresponding XRD patterns.

The growth mechanism of nanowires

To better understand the growth mechanism of wurtzite $CuGaS_2$ nanowires, the products collected at different reaction temperatures in OLA were characterized by TEM and XRD as shown in Figure 9. The nucleation and growth of nanowires were highly dependent on reaction temperatures. In the first step, small $CuGaS_2$ nuclei were formed at 130 ^oC (Figure 9a). Even though the reaction time was prolonged to 1 hr, no wire-like nanocrystals can be found in the product. $CuGaS_2$ nanparticles aggregated together when temperature was raised to 180 ^oC (Figure 9b). Nanowires were formed by increasing the reaction temperature to 200 ^oC. Rearrangement of the short $CuGaS_2$ nanowires in the length range of 100 nm to 1 μm was observed (Figure 9c). The growth of $CuGaS_2$ nanocrystals could be due to oriented attachment and Ostwald ripening.[46] In Figure 9d, the further growth of the $CuGaS_2$ nanowire took place while the reaction temperature was increased to 240 ^oC. The nanowires collected at 240 ^oC for 5 min have the length ranging from 100 nm to 4 μm. The XRD characterization (Figure 9e) was conducted of various growth stages and

Table 2. Experimental parameters and their results

Figure No.	Sulfur source	Stabilizing agents, Solvent	Reaction Temp. (°C)	Crystalline phase	Morphology
Figure 2	sulfur	OLA (12 mL)	240	chalcopyrite	nanoparticles (5-11 nm)
Figure 3	sulfur	OLA(8 mL), DDT (4 mL)	180	chalcopyrite	3 nm nanoparticles
Figure 5	thiourea	OLA (24 mL)	240	wurtzite	nanoparticles (29.9±6.6 nm)
Figure 6	thiourea	OLA (12 mL)	240	wurtzite	nanowires
Figure 7	thiourea	DDA (12 mL)	240	wurtzite	aggregated nanopartices (5-8 nm)

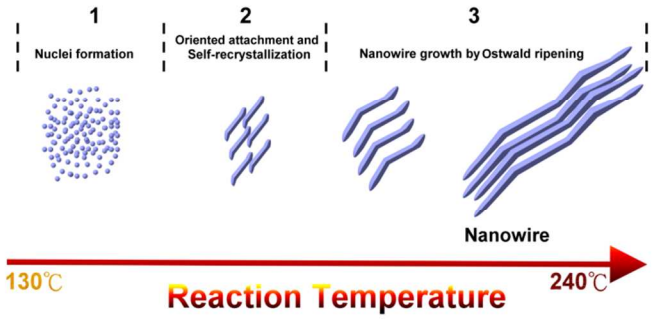

Scheme 1. Schematic illustration of the growth mechanism of the obtained wurtzite $CuGaS_2$ Nanowire.

reveals that all products are wurtzite structure of $CuGaS_2$. Interestingly, (002) reflection observed in the XRD patterns become stronger with increasing the reaction temperature, but other peaks reflection increase slower without changing the position of peaks. The result suggests that the $CuGaS_2$ nanowires are preferentially oriented and (002) peak. The relationship between the reaction temperature and the morphology evolution of $CuGaS_2$ nanowires is summarized as a schematic diagram (scheme 1).

4. Conclusions

In summary, we have developed a systematic synthetic approach to obtain different sizes, phases, shapes of $CuGaS_2$ nanocrystals. Different sizes of chalcopyrite $CuGaS_2$ nanoparticles exhibit the size-dependent optical properties consistent with theoretical calculation. The sulfur source plays pivotal roles in crystal phase determination: sulfur powder leads to chaocopyrite $CuGaS_2$ and thiourea leads to wurtzite phase. In the synthesis of wurtzite $CuGaS_2$, smaller amount of OLA promotes anisotropic growth. It was observed that the formation of these nanowires through oriented attachment accompany with Ostwald ripening by observing the morphology evolution of products from 130 °C to 240 °C. This results show a different synthetic path to obtain I-III-VI group of nanowires compared with existing examples for ternary nanowires grown by vapor-liquid-solid method (VLS), solution-liquid-solid method (SLS) and phase transformation mechanisms.

Acknowledgements

The authors acknowledge the financial support by the National Science Council of Taiwan (NSC 102-2221-E-007-023-MY3, NSC 102-2221-E-007-090-MY2, and NSC 101-2623-E-007-013-IT), the Minitry of Economic Affairs, Taiwan (101-EC-17-A-09-S1-198), National Tsing Hua University (102N2051E1, 102N2061E1), and the assistance from Center for Energy and Environmental Research, National Tsing-Hua University.

Notes and references

Department of Chemical Engineering, National Tsing Hua University, 101, Section 2, Kuang-Fu Road, Hsinchu, Taiwan 30013, ROC. E-mail: hytuan@che.nthu.edu.tw, Tel.: +886-3-572-3661. Fax: +886-3-571-5408.

† Author Contributions: These authors contributed equally. Electronic Supplementary Information (ESI) available: EDS data are shown in the supplementary information. See DOI: 10.1039/b000000x/

References

1. J. Xu, C. S. Lee, Y. B. Tang, X. Chen, Z. H. Chen, W. J. Zhang, S. T. Lee, W. X. Zhang and Z. H. Yang, *ACS Nano*, 2010, **4**, 1845-1850.
2. W. E. Devaney, W. S. Chen, J. M. Stewart and R. A. Mickelsen, *IEEE T. Electron Dev.*, 1990, **37**, 428-433.
3. R. Scheer, T. Walter, H. W. Schock, M. L. Fearheiley and H. J. Lewerenz, *Appl. Phys. Lett.*, 1993, **63**, 3294-3296.
4. V. A. Akhavan, B. W. Goodfellow, M. G. Panthani, D. K. Reid, D. J. Hellebusch, T. Adachi and B. A. Korgel, *Energy Environ. Sci.*, 2010, **3**, 1600-1606.
5. H. Ye, H. S. Park, V. A. Akhavan, B. W. Goodfellow, M. G. Panthani, B. A. Korgel and A. J. Bard, *J. Phys. Chem. C*, 2010, **115**, 234-240.
6. Q. Guo, S. J. Kim, M. Kar, W. N. Shafarman, R. W. Birkmire, E. A. Stach, R. Agrawal and H. W. Hillhouse, *Nano lett.*, 2008, **8**, 2982-2987.
7. Q. Guo, G. M. Ford, H. W. Hillhouse and R. Agrawal, *Nano lett.*, 2009, **9**, 3060-3065.
8. W. Liu, D. B. Mitzi, M. Yuan, A. J. Kellock, S. J. Chey and O. Gunawan, *Chem. Mater.*, 2009, **22**, 1010-1014.
9. M.-Z. Xue and Z.-W. Fu, *Thin Solid Films*, 2008, **516**, 8386-8392.
10. W. Zhang, H. Zeng, Z. Yang and Q. Wang, *J. Solid State Chem.*, 2012, **186**, 58-63.
11. M. G. Panthani, T. A. Khan, D. K. Reid, D. J. Hellebusch, M. R. Rasch, J. A. Maynard and B. A. Korgel, *Nano Lett.*, 2013, **13**, 4294-4298.
12. C. J. Hibberd, E. Chassaing, W. Liu, D. B. Mitzi, D. Lincot and A. N. Tiwari, *Prog. Photovoltaics*, 2010, **18**, 434-452.

13. Y. G. Cai, J. C. W. Ho, S. K. Batabyal, W. Liu, Y. Sun, S. G. Mhaisalkar and L. H. Wong, *ACS Appl. Mater. Interfaces*, 2013, **5**, 1533-1537.
14. M. G. Panthani, V. Akhavan, B. Goodfellow, J. P. Schmidtke, L. Dunn, A. Dodabalapur, P. F. Barbara and B. A. Korgel, *J. Am. Chem. Soc.*, 2008, **130**, 16770-16777.
15. V. A. Akhavan, B. W. Goodfellow, M. G. Panthani, C. Steinhagen, T. B. Harvey, C. J. Stolle and B. A. Korgel, *J. Solid State Chem.*, 2012, **189**, 2-12.
16. S.-H. Chang, M.-D. Lu, Y.-L. Tung and H.-Y. Tuan, *ACS Nano*, 2013, **7**, 9443-9451.
17. Y.-G. Chun, K.-H. Kim and K.-H. Yoon, *Thin Solid Films*, 2005, **480**, 46-49.
18. W.-C. Huang, C.-H. Tseng, S.-H. Chang, H.-Y. Tuan, C.-C. Chiang, L.-M. Lyu and M. H. Huang, *Langmuir*, 2012, **28**, 8496-8501.
19. W. H. Hsu, H. I. Hsiang, Y. L. Chang, D. T. Ray and F. S. Yen, *J. Am. Ceram. Soc.*, 2011, **94**, 3030-3034.
20. B. Koo, R. N. Patel and B. A. Korgel, *Chem. Mater.*, 2009, **21**, 1962-1966.
21. M.-Y. Chiang, S.-H. Chang, C.-Y. Chen, F.-W. Yuan and H.-Y. Tuan, *J. Phys. Chem. C*, 2011, **115**, 1592-1599.
22. S.-H. Chang, M.-Y. Chiang, C.-C. Chiang, F.-W. Yuan, C.-Y. Chen, B.-C. Chiu, T.-L. Kao, C.-H. Lai and H.-Y. Tuan, *Energy Environ. Sci.*, 2011, **4**, 4929-4932.
23. Q. Li, L. Zhai, C. Zou, X. Huang, L. Zhang, Y. Yang, X. a. Chen and S. Huang, *Nanoscale*, 2013, **5**, 1638-1648.
24. A. J. Wooten, D. J. Werder, D. J. Williams, J. L. Casson and J. A. Hollingsworth, *J. Am. Chem. Soc.*, 2009, **131**, 16177-16188.
25. M. Kruszynska, H. Borchert, A. Bachmatiuk, M. H. Ru□mmeli, B. Bu□chner, J. r. Parisi and J. Kolny-Olesiak, *ACS Nano*, 2012, **6**, 5889-5896.
26. O. Yarema, D. Bozyigit, I. Rousseau, L. Nowack, M. Yarema, W. Heiss and V. Wood, *Chem. Mater.*, 2013, **25**, 3753-3757.
27. J. Hu, L.-s. Li, W. Yang, L. Manna, L.-w. Wang and A. P. Alivisatos, *Science*, 2001, **292**, 2060-2063.
28. Y. N. Xia, P. D. Yang, Y. G. Sun, Y. Y. Wu, B. Mayers, B. Gates, Y. D. Yin, F. Kim and Y. Q. Yan, *Adv. Mater.*, 2003, **15**, 353-389.
29. Z. Tang and N. A. Kotov, *Adv. Mater.*, 2005, **17**, 951-962.
30. M. Giersig, I. Pastoriza-Santos and L. M. Liz-Marzan, *J. Mater. Chem.*, 2004, **14**, 607-610.
31. K.-S. Cho, D. V. Talapin, W. Gaschler and C. B. Murray, *J. Am. Chem. Soc.*, 2005, **127**, 7140-7147.
32. C. Pacholski, A. Kornowski and H. Weller, *Angew. Chem.-Int. Edit.*, 2002, **41**, 1188-1191.
33. X. Lu, Z. Zhuang, Q. Peng and Y. Li, *Crystengcomm*, 2011, **13**, 4039-4045.
34. F. Wang, Y. Han, C. S. Lim, Y. H. Lu, J. Wang, J. Xu, H. Y. Chen, C. Zhang, M. H. Hong and X. G. Liu, *Nature*, 2010, **463**, 1061-1065.
35. Y. H. A. Wang, X. Y. Zhang, N. Z. Bao, B. P. Lin and A. Gupta, *J. Am. Chem. Soc.*, 2011, **133**, 11072-11075.
36. S. Levcenko, N. Syrbu, V. Tezlevan, E. Arushanov, S. Doka-Yamigno, T. Schedel-Niedrig and M. C. Lux-Steiner, *J. Phys.-Condes. Matter*, 2007, **19**, 456222.
37. M. D. Regulacio, C. Ye, S. H. Lim, Y. Zheng, Q. Xu and M. Han, *Crystengcomm*, 2013, **15**, 5214-5217.
38. J. Hu, B. Deng, C. Wang, K. Tang and Y. Qian, *Solid State Commun.*, 2002, **121**, 493-496.
39. Q. Lu, J. Hu, K. Tang, Y. Qian, G. Zhou and X. Liu, *Inorg. Chem.*, 2000, **39**, 1606-1607.
40. Q. Li, C. Zou, L. Zhai, J. Shen, L. Zhang, H. Yu, Y. Yang, X. a. Chen and S. Huang, *J. Alloy. Compd.*, 2013, **567**, 127-133.
41. K. Nose, Y. Soma, T. Omata and S. Otsuka-Yao-Matsuo, *Chem. Mater.*, 2009, **21**, 2607-2613.
42. D. C. Pan, L. J. An, Z. M. Sun, W. Hou, Y. Yang, Z. Z. Yang and Y. F. Lu, *J. Am. Chem. Soc.*, 2008, **130**, 5620-5621.
43. G. D. Scholes, H. Z. Zhong, S. S. Lo, T. Mirkovic, Y. C. Li, Y. Q. Ding and Y. F. Li, *ACS Nano*, 2010, **4**, 5253-5262.
44. D. Aldakov, A. Lefrançois and P. Reiss, *J. Mater. Chem. C*, 2013, **1**, 3756-3776.
45. T. Omata, K. Nose and S. Otsuka-Yao-Matsuo, *J. Appl. Phys.*, 2009, **105**, 073106-073106-073105.
46. H. Zhong, Y. Zhou, M. Ye, Y. He, J. Ye, C. He, C. Yang and Y. Li, *Chem. Mater.*, 2008, **20**, 6434-6443.